Publication V

Piippo, A. and Luomi, J. (2006). "Torque ripple reduction in sensorless PMSM drives." In *Proceedings of The 32nd Annual Conference of the IEEE Industrial Electronics Society (IECON'06)*, pp. 920–925, Paris, France.

Torque Ripple Reduction in Sensorless PMSM Drives

Antti Piippo and Jorma Luomi
Power Electronics Laboratory
Helsinki University of Technology
P.O. Box 3000, FI-02015 TKK, Finland

***Abstract*— The paper proposes a method for the compensation of the torque ripple that is caused by motor unidealities in sensorless permanent magnet synchronous motor drives. The sensorless control of the interior-magnet motor is based on a speed-adaptive observer augmented with a pulsating high-frequency signal injection technique at low speeds. The harmonics in the permanent magnet flux and stator inductances are taken into account in the estimation, and a torque ripple compensator is developed for suppressing the harmonics in the estimated electromagnetic torque. The high-bandwidth current control required for torque ripple reduction is based on additional PI controllers implemented in reference frames rotating at the harmonic frequencies. Simulations and laboratory experiments show the effectiveness of the proposed method.**

I. Introduction

Permanent magnet synchronous machines (PMSMs) are used in many high-performance applications. The absence of the magnetizing current and negligible rotor losses lead to a high torque-to-weight ratio and a good efficiency. Unidealities in the motor cause ripple in the electromagnetic torque and, in the case of position-sensorless control, errors in the rotor speed and position estimation. The torque ripple can be minimized by proper motor design—in some cases with the expense of the torque-to-weight ratio—but the remaining torque pulsations can still deteriorate the performance of the motor drive. Therefore, significant research efforts have been put on suppressing the torque ripple, principally by modifying the stator current waveforms [1].

The torque ripple has several origins. Unidealities in the rotor geometry cause a nonsinusoidal air-gap distribution of the permanent magnet flux and thus a nonsinusoidal variation of the back-emf. The rotor geometry and the nonsinusoidal distribution of the stator mmf produce spatial harmonics in the stator inductances. These phenomena cause load-dependent periodic ripple in the electromagnetic torque [2]. Slotting effects can produce a cogging torque, which is independent on the stator current. In addition, unidealities in the inverter and measurements can cause torque ripple.

Surface-magnet machines do not have pronounced magnetic saliency, and spatial harmonics in the back-emf are the primary cause of load-dependent torque ripple. Various methods have been proposed for compensating the torque ripple [3]–[8]. In [3], the torque ripple generated by flux harmonics and slotting effects is compensated. The flux harmonics are determined by a self-commissioning scheme and used to modify the current reference trajectory. An MRAS-type torque estimator and an integral variable-structure torque controller are used in [4]. Optimal current waveforms are derived for surface-magnet PMSMs in [5], considering both current minimization and optimal torque. An adaptive controller for minimizing the torque ripple is presented in [6], and simple expressions for current references are derived in [7]. A repetitive current controller for tracking periodic current references is proposed in [8].

Methods for compensating the torque ripple have also been proposed for interior-magnet machines, which have magnetic saliency [2], [9]–[11]. In these machines, the contribution of the inductance harmonics to the torque ripple should also be taken into account [10]. The current references can be determined on-line by controlling the estimated torque [2], [11]. The reluctance torque should also be taken into account for obtaining optimum current references; off-line calculation of current waveforms has been used for this purpose [9], [10]. However, it is more straightforward and flexible to implement an on-line torque controller. It is to be noted that a position measurement is used in all the previous methods.

This paper proposes a method for the compensation of the torque ripple of an interior-magnet PMSM in sensorless operation. The sensorless control is based on a speed-adaptive observer augmented with a pulsating high-frequency signal injection technique at low speeds [12]. Both the flux harmonics and the inductance harmonics are taken into account in the estimation of the torque, speed, and position. A torque ripple compensator is proposed for suppressing the estimated torque harmonics, and a current-minimizing method is used for evaluating the d-q current references. In addition to the PI control of the fundamental current, the current harmonics are controlled by PI controllers implemented in reference frames rotating at the harmonic frequencies. Simulation and experimental results are shown at the end of the paper.

II. PMSM Model

The PMSM is modeled in the d-q reference frame fixed to the rotor. The d axis is oriented along the permanent magnet flux, whose angle in the stator reference frame is θ_m in electrical radians. The stator voltage equation is

$$\mathbf{u}_s = R_s \mathbf{i}_s + \dot{\boldsymbol{\psi}}_s + \omega_m \mathbf{J} \boldsymbol{\psi}_s \tag{1}$$

where $\mathbf{u}_s = [\, u_d \;\; u_q \,]^T$ is the stator voltage, $\mathbf{i}_s = [\, i_d \;\; i_q \,]^T$ the stator current, $\boldsymbol{\psi}_s = [\, \psi_d \;\; \psi_q \,]^T$ the stator flux, R_s the stator resistance, $\omega_m = \dot{\theta}_m$ the electrical angular speed of the rotor, and

$$\mathbf{J} = \begin{bmatrix} 0 & -1 \\ 1 & 0 \end{bmatrix}$$

1-4244-0136-4/06/$20.00 ©2006 IEEE

The stator flux is

$$\boldsymbol{\psi}_s = \mathbf{L}\mathbf{i}_s + \boldsymbol{\psi}_{pm} \tag{2}$$

where $\boldsymbol{\psi}_{pm}$ is the permanent magnet flux and $\mathbf{L}$ is the inductance matrix.

When the rotor position angle θ_m is varied, the permanent magnet flux linkages of the three stator winding phases consist of a fundamental component and odd harmonics. In the d-q reference frame, the permanent magnet flux has a constant component ψ_{pm0} on the d axis and harmonics of orders multiple of six. For simplicity, the harmonics having orders higher than six are omitted in this paper, resulting in the permanent magnet flux vector [2]

$$\boldsymbol{\psi}_{pm} = \begin{bmatrix} \psi_{pm0} + \psi_{d6}\cos(6\theta_m) \\ \psi_{q6}\sin(6\theta_m) \end{bmatrix} \tag{3}$$

where ψ_{d6} and ψ_{q6} are the coefficients of the sixth-order harmonics on the d and q axes, respectively.

The self and mutual inductances of the stator winding phases have an average component and even harmonics when the rotor position angle is varied. In the d-q reference frame, the inductance matrix consists of the direct-axis inductance L_d and quadrature-axis inductance L_q on the d and q axes, respectively, and harmonics of orders multiple of six. When the higher-order harmonics are omitted, the stator inductance matrix is [2]

$$\mathbf{L} = \begin{bmatrix} L_d + L_6\cos(6\theta_m) & -L_6\sin(6\theta_m) \\ -L_6\sin(6\theta_m) & L_q - L_6\cos(6\theta_m) \end{bmatrix} \tag{4}$$

where L_6 is the amplitude of the sixth harmonic of the stator inductance.

The electromagnetic torque can be obtained by differentiating the magnetic co-energy with respect to the rotor position. The result is [10]

$$\begin{aligned} T_e = \frac{3p}{2}\{&\psi_{pm0}i_q + (L_d - L_q)i_d i_q \\ &- 2L_6\sin(6\theta_m)(i_d^2 - i_q^2) \\ &- 4L_6\cos(6\theta_m)i_d i_q \\ &+ i_q\cos(6\theta_m)(\psi_{d6} + 6\psi_{q6}) \\ &- i_d\sin(6\theta_m)(\psi_{q6} + 6\psi_{d6})\} \end{aligned} \tag{5}$$

where p is the number of pole pairs.

III. Sensorless Control Using an Adaptive Observer

In the adaptive observer, the stator flux is estimated with two models, and the estimate of the rotor speed is used for adjusting the adaptive model [12]. For including the harmonics in the estimation, the definitions (3) and (4) are used for the permanent magnet flux vector and the stator inductance matrix, respectively [13]. The observer is formulated in the estimated rotor reference frame.

The block diagram of the adaptive observer is shown in Fig. 1. The reference model is based on (2); this flux model can be written as

$$\hat{\boldsymbol{\psi}}_{s,i} = \hat{\mathbf{L}}\mathbf{i}'_s + \hat{\boldsymbol{\psi}}_{pm} \tag{6}$$

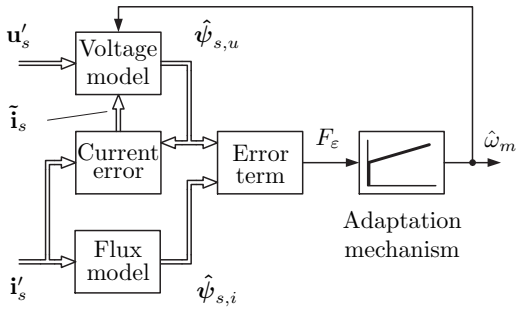

Fig. 1. Block diagram of the adaptive observer.

Estimated quantities are marked by $\hat{}$, and measured quantities expressed in the estimated rotor reference frame by $'$. The adaptive model is based on (1) and (2). It is here referred to as a voltage model, and defined by

$$\dot{\hat{\boldsymbol{\psi}}}_{s,u} = \mathbf{u}'_s - \hat{R}_s\hat{\mathbf{i}}_s - \hat{\omega}_m\mathbf{J}\hat{\boldsymbol{\psi}}_{s,u} + \boldsymbol{\lambda}\tilde{\mathbf{i}}_s \tag{7}$$

where the estimate of the stator current and the estimation error of the stator current are

$$\hat{\mathbf{i}}_s = \hat{\mathbf{L}}^{-1}(\hat{\boldsymbol{\psi}}_{s,u} - \hat{\boldsymbol{\psi}}_{pm}) \tag{8}$$

$$\tilde{\mathbf{i}}_s = \mathbf{i}'_s - \hat{\mathbf{i}}_s \tag{9}$$

respectively. The feedback gain matrix $\boldsymbol{\lambda}$ is varied as a function of the rotor speed [14].

The adaptation is based on the error term

$$F_\varepsilon = \mathbf{C}_1\tilde{\boldsymbol{\psi}}_s \tag{10}$$

where $\tilde{\boldsymbol{\psi}}_s = \hat{\boldsymbol{\psi}}_{s,i} - \hat{\boldsymbol{\psi}}_{s,u}$ is the difference between the flux estimates, and $\mathbf{C}_1 = [\,0\;\;1\,]$. Hence the flux difference in the estimated q direction is used. The estimate of the electrical angular speed of the rotor, used in (7), is obtained by a PI speed adaptation mechanism from F_ε. The estimate $\hat{\theta}_m$ for the rotor position is evaluated by integrating $\hat{\omega}_m$. At low speeds, the adaptive observer is augmented with a high-frequency (HF) signal injection method [12]. A modified HF voltage signal is used for compensating the estimation error caused by the inductance harmonics [13].

IV. Torque and Current Regulation

The principle selected for torque ripple reduction is to suppress individual harmonics in the estimated torque. The block diagram of the torque and current control loops is shown in Fig. 2.

A. Torque Harmonics Suppression

Eq. (5) is applied for the torque estimation. The stator current is predicted one sampling time step ahead [15] to compensate the delay in the measured current. The harmonics in the permanent-magnet flux and in the stator inductances are taken into account in the stator current prediction.

The estimated electromagnetic torque is first low-pass filtered by

$$\dot{\hat{T}}_{e,av} = \alpha_{lp,T}|\hat{\omega}_m/\omega_B|(\hat{T}_e - \hat{T}_{e,av}) \tag{11}$$

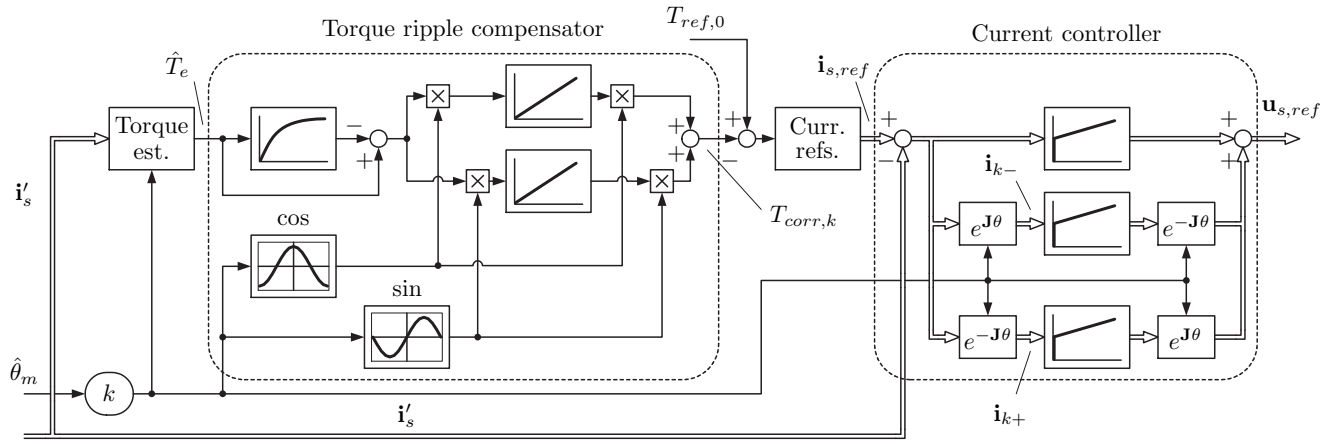

Fig. 2. Block diagram of torque ripple compensator and current controller. Gain k denotes order of harmonic to be compensated and $T_{ref,0}$ is fundamental torque reference.

where $\alpha_{lp,T}$ is the low-pass filter bandwidth at the base speed ω_B. The low-pass filtered torque estimate is used for calculating the high-frequency part $\hat{T}_e - \hat{T}_{e,av}$ of the estimated torque. From the high-frequency part, signals representing the harmonic components of the torque estimate are evaluated as

$$T_{ka} = 2(\hat{T}_e - \hat{T}_{e,av})\cos(k\hat{\theta}_m) \tag{12a}$$

$$T_{kb} = 2(\hat{T}_e - \hat{T}_{e,av})\sin(k\hat{\theta}_m) \tag{12b}$$

where k is the order of the torque ripple harmonic. The average values of these signals are the coefficients of the Fourier series in steady state. The harmonic components of $\hat{T}_e$ are controlled to zero by integral controllers

$$\dot{T}_{ka,i} = \alpha_{lp,T}|\hat{\omega}_m/\omega_B|T_{ka} \tag{13a}$$

$$\dot{T}_{kb,i} = \alpha_{lp,T}|\hat{\omega}_m/\omega_B|T_{kb} \tag{13b}$$

The outputs of these controllers are used for calculating a torque correction

$$T_{corr,k} = T_{ka,i}\cos(k\hat{\theta}_m) + T_{kb,i}\sin(k\hat{\theta}_m) \tag{14}$$

which is subtracted from the electromagnetic torque reference $T_{ref,0}$.

In steady state, the integration in (13) results in the suppression of the specific harmonic in the electromagnetic torque estimate. Several harmonics can be suppressed by repeating (12)–(14) for different values of k. Since the ripple amplitudes decay when k increases, it is reasonable to suppress only one or two of the lowest-order harmonics. For simplicity, only the sixth harmonic ($k = 6$) is suppressed in this paper.

B. High-Frequency Current Regulation

From the modified torque reference that includes harmonics, the d and q components of the current reference $\mathbf{i}_{s,ref}$ are calculated according to maximum-torque-per-current control [16]. Hence, both the d and q components contain harmonics. The flux and inductance harmonics are not taken into account in the current reference calculation.

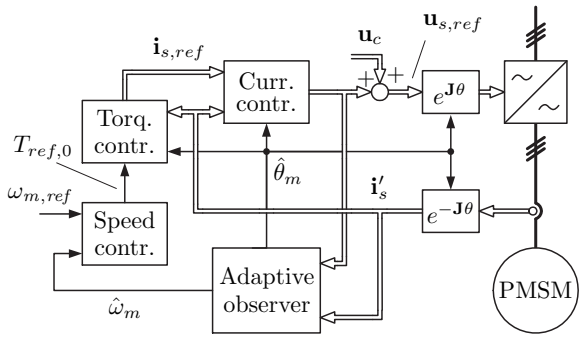

Fig. 3. Block diagram of the control system. $\mathbf{u}_c$ is the HF carrier excitation signal of the signal injection method.

The current harmonics are controlled using a dual current control method [17] in parallel with the PI control of the fundamental current. The current error term is transformed to reference frames rotating at the angular frequency $k\hat{\omega}_m$ both in the positive direction ($\mathbf{i}_{k+}$) and in the negative direction ($\mathbf{i}_{k-}$) with respect to the estimated rotor position. In the rotating reference frames, the current error terms are low-pass filtered to extract the harmonic current error of the order k,

$$\dot{\mathbf{i}}_{k+,av} = \alpha_{lp,i}|\hat{\omega}_m/\omega_B|(\mathbf{i}_{k+} - \mathbf{i}_{k+,av}) \tag{15a}$$

$$\dot{\mathbf{i}}_{k-,av} = \alpha_{lp,i}|\hat{\omega}_m/\omega_B|(\mathbf{i}_{k-} - \mathbf{i}_{k-,av}) \tag{15b}$$

where $\alpha_{lp,i}$ is the low-pass filter bandwidth at the base speed. After the filtering, ordinary PI control is used for the regulation of each harmonic current error. The outputs of the PI controllers are transformed back to the rotor reference frame, where they are added to the fundamental voltage reference. For clarity, the current filtering is omitted in Fig. 2—and so is the decoupling of cross-coupling terms and back-emf [18].

V. Simulation Results

The proposed method was investigated by means of simulations and laboratory experiments. Fig. 3 shows the block diagram of the control system comprising cascaded speed

TABLE I

MOTOR DATA

Nominal voltage U_N	370 V
Nominal current I_N	4.3 A
Nominal frequency f_N	75 Hz
Nominal torque T_N	14.0 Nm
Stator resistance R_s	3.59 Ω
Direct-axis inductance L_d	36.0 mH
Quadrature-axis inductance L_q	51.0 mH
Inductance harmonic amplitude L_6	1.1 mH
Permanent magnet flux ψ_{pm0}	0.545 Vs
Flux harmonic coefficient ψ_{d6}	−1.0 mVs
Flux harmonic coefficient ψ_{q6}	1.4 mVs
Total moment of inertia	0.015 kgm^2

TABLE II

CONTROL SYSTEM PARAMETERS

Current controller bandwidth	2π·400 rad/s
Speed controller bandwidth	2π·5 rad/s
Bandwidth $\alpha_{lp,T}$	2π·15 rad/s
Bandwidth $\alpha_{lp,i}$	2π·37.5 rad/s

and current control loops. PI-type speed control with active damping is used. The data of the six-pole interior-magnet PMSM (2.2 kW, 1500 rpm) are given in Table I. The base values for voltage, current, and angular speed are defined as $U_B = \sqrt{2/3}U_N$, $I_B = \sqrt{2}I_N$, and $\omega_B = 2\pi f_N$, respectively. The electromagnetic torque is limited to 22 Nm, which is 1.57 times the nominal torque T_N. The high-frequency carrier excitation signal has a frequency of 833 Hz and an amplitude of 40 V. The HF signal injection is used below speed 0.13 p.u. Other parameters of the control system are given in Table II.

The MATLAB/Simulink environment was used for the simulations. The parameter values used in the controller were equal to those of the motor model. Fig. 4 shows results obtained in steady state when the speed reference is 0.5 p.u. and load torque is at the nominal value. In the original method shown in Fig. 4(a), the torque ripple compensation and the sixth harmonic current control are not used. Although the q-axis current reference is nearly constant, a significant sixth harmonic is present in the actual current and torque because of the harmonics in the motor. In the proposed method shown in Fig. 4(b), the torque ripple compensation and the sixth harmonic current control have been added to the control system. The current follows the sixth harmonic of the current reference, which is generated by the torque ripple compensator, and the sixth harmonic is suppressed in the electromagnetic torque.

The estimated torque follows the actual torque with a good accuracy in the previous examples, the current prediction being an essential part of the estimation. Without the prediction, the delay in the measured current would cause an error that increases with the rotor speed, thus degrading the performance of the torque ripple compensation.

Fig. 5 shows the rotor speed and the electromagnetic torque during an acceleration from $\omega_m = 0.2$ p.u. to $\omega_m = 0.6$ p.u. at the nominal load torque for the original method and for the proposed method. By comparing Figs. 5(a) and 5(b), it can be seen that a sixth harmonic appears in the torque, but the torque

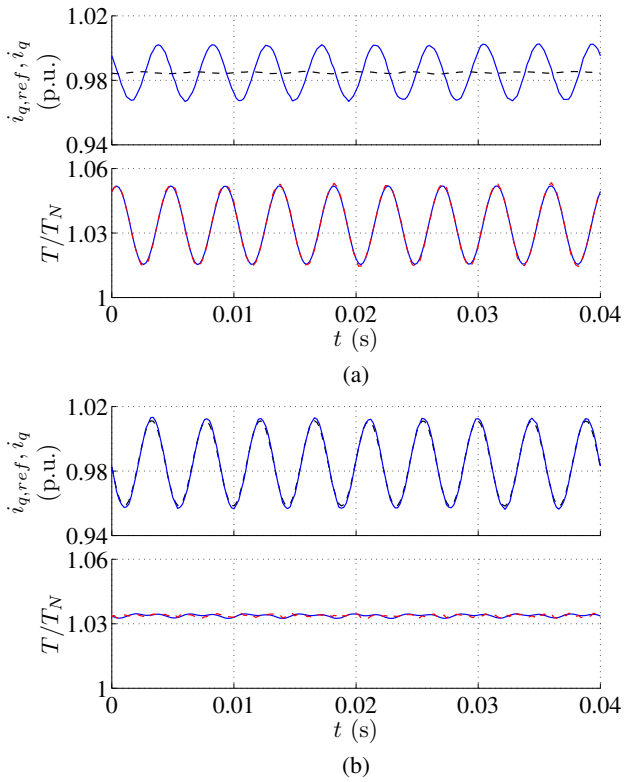

Fig. 4. Simulation results showing steady-state operation: (a) original method (b) proposed method. Speed reference is 0.5 p.u. and load torque is at nominal value. First subplot shows q-axis current in the estimated rotor reference frame (solid) and its reference (dashed). Second subplot shows electromagnetic torque (solid) and its estimate (dashed)

ripple compensator reduces it already during the acceleration. When the speed settles to $\omega_m = 0.6$ p.u., the sixth harmonic is almost completely suppressed in the torque. Since the torque ripple is dependent on the stator current, the ripple increases with load at $t = 0.1$ s in Fig. 5(b) and is reduced again after the transient. Improving the dynamic performance of the torque ripple compensation by increasing the bandwidth $\alpha_{lp,T}$ can result in oscillatory behavior in fast transients or even in steady state. The selection of the $\alpha_{lp,T}$ is thus a trade-off between dynamic performance and steady-state accuracy.

VI. EXPERIMENTAL RESULTS

The experimental setup is illustrated in Fig. 6. The PMSM is fed by a frequency converter that is controlled by a dSPACE DS1103 PPC/DSP board. Mechanical load is provided by a PMSM servo drive. An incremental encoder is used for monitoring the actual rotor speed and position. The nominal dc-link voltage is 540 V, and the switching frequency and the sampling frequency are both 5 kHz. The dc-link voltage of the converter is measured, and a simple current feedforward compensation for dead times and power device voltage drops is applied [19].

Fig. 7 shows experimental results in steady-state operation, corresponding to the simulation in Fig. 4. In addition to the sixth harmonic, lower-order harmonics are present in the current and torque. When the proposed method is used, the

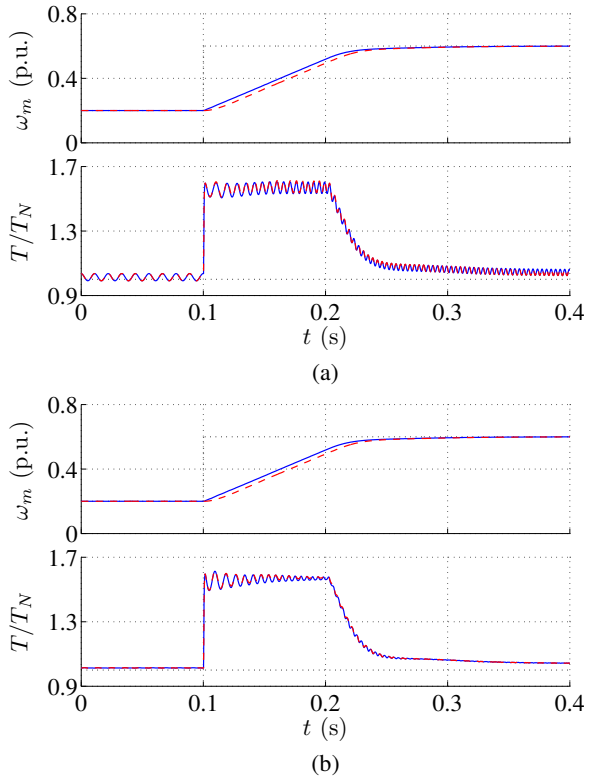

Fig. 5. Simulation results showing speed reference step at t = 0.1 s: (a) original method (b) proposed method. Load torque is at nominal value. First subplot shows electrical angular speed of the rotor (solid), its estimate (dashed) and its reference (dotted). Second subplot shows load torque reference (dotted), electromagnetic torque (solid) and its estimate (dashed).

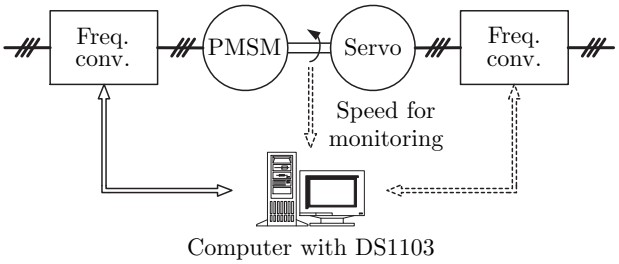

Fig. 6. Experimental setup. Mechanical load is provided by a servo drive.

actual q-axis current follows the sixth harmonic in the current reference, and the sixth harmonic in the electromagnetic torque estimate is considerably reduced as compared with the original method. Fig. 8 shows experimental results for the acceleration considered in Fig. 5. The ripple reduction in the estimated electromagnetic torque is visible, but some lower-order harmonics remain in the estimated torque.

Experimental results during a slow speed reversal are shown in Fig. 9 for the original method and for the proposed method. The speed reference changes from 0.33 p.u. to -0.33 p.u. between $t = 2$ s and $t = 28$ s and load torque is at the nominal value between $t = 1$ s and $t = 29$ s. Again, the reduction of the sixth-harmonic ripple is visible. The proposed method is not in use at low speeds ($|\omega_m| < 0.05$ p.u.) since it would deteriorate the dynamic performance. Therefore, the

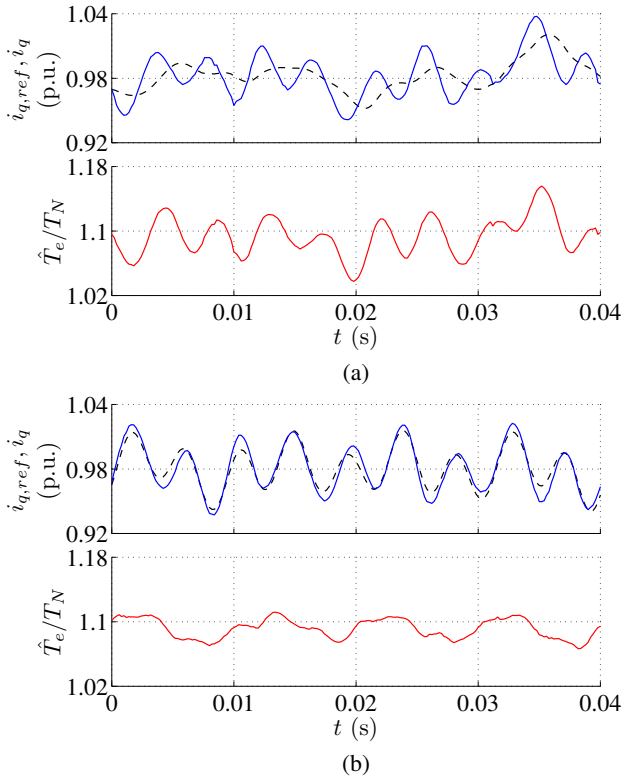

Fig. 7. Experimental results showing steady-state operation: (a) original method (b) proposed method. Speed reference is 0.5 p.u. and load torque is at nominal value. First subplot shows q-axis current in the estimated rotor reference frame (solid) and its reference (dashed). Second subplot shows estimated electromagnetic torque

ripple remains in the estimated torque in the low-speed region. Torque ripple compensation is not necessarily needed at very low speeds, since the speed control loop reduces the ripple.

VII. Conclusions

The method proposed for torque ripple reduction is suitable for sensorless PMSM drives. Both flux harmonics and inductance harmonics are taken into account, and a harmonic in the torque estimate is suppressed using a torque ripple compensator based on three additional motor parameters. The current control is augmented with a dual current control method, allowing control of high-frequency harmonics. Identification of the parameters required in the torque estimation is a suitable future research topic. Simulations and laboratory experiments show the effectiveness of the proposed method.

Acknowledgement

The authors gratefully acknowledge the financial support given by ABB Oy and Walter Ahlström foundation.

References

[1] T. Jahns and W. Soong, "Pulsating torque minimization techniques for permanent-magnet AC motor drives—a review," *IEEE Trans. Ind. Electron.*, vol. 43, no. 2, pp. 321–330, April 1996.

[2] T. S. Low, K. J. Tseng, T. H. Lee, K. W. Lim, and K. S. Lock, "Strategy for the instantaneous torque control of permanent-magnet brushless DC drives," *IEE Proc. B, Elect. Power Appl.*, vol. 137, no. 6, pp. 355–363, Nov. 1990.

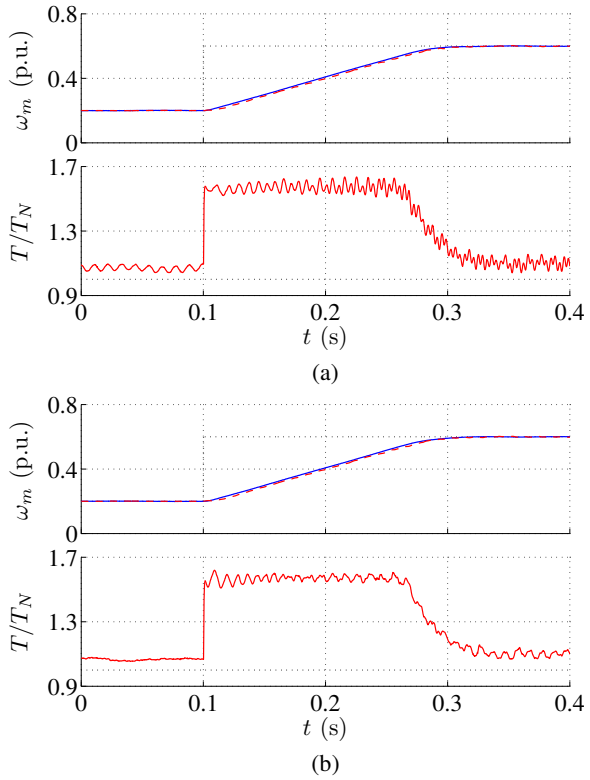

Fig. 8. Experimental results showing speed reference step at t = 0.1 s: (a) original method (b) proposed method. Load torque is at nominal value. First subplot shows electrical angular speed of the rotor (solid), its estimate (dashed) and its reference (dotted). Second subplot shows load torque reference (dotted) and electromagnetic torque estimate (solid).

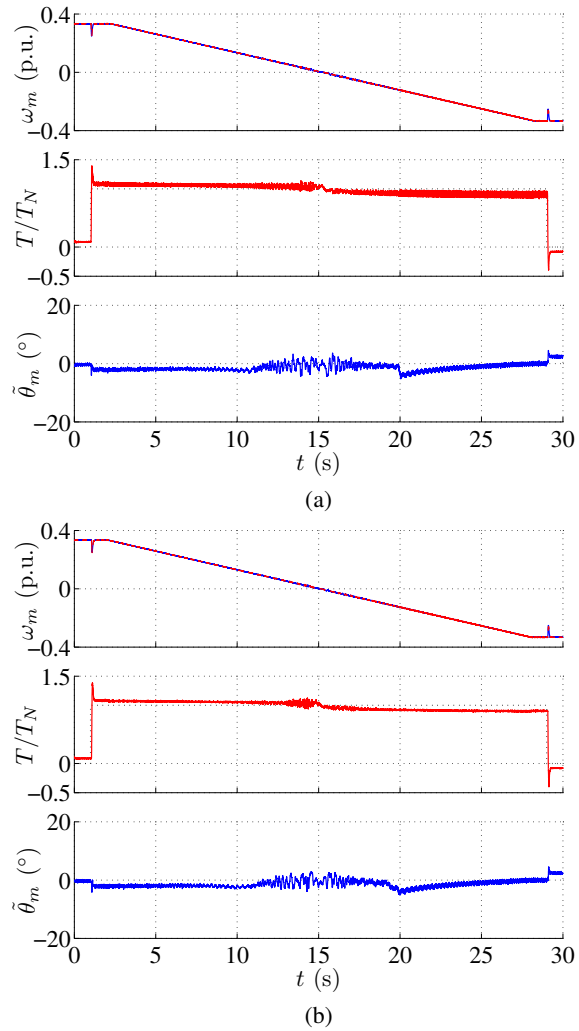

Fig. 9. Experimental results showing slow speed reversal at nominal load torque: (a) original method (b) proposed method. First subplot shows electrical angular speed (solid), its estimate (dashed), and its reference (dotted). Second subplot shows estimated electromagnetic torque (solid) and load torque reference (dotted). Last subplot shows estimation error of rotor position in electrical degrees.

[3] J. Holtz and L. Springob, "Identification and compensation of torque ripple in high-precision permanent magnet motor drives," *IEEE Trans. Ind. Electron.*, vol. 43, no. 2, pp. 309–320, Apr. 1996.

[4] S. Chung, H. Kim, C. Kim, and M. Youn, "A new instantaneous torque control of PM synchronous motor for high performance direct drive applications," *IEEE Trans. Pow. Electron.*, vol. 13, no. 3, pp. 388–400, May 1998.

[5] P. L. Chapman, S. D. Sudhoff, and C. A. Whitcomb, "Optimal current control strategies for surface-mounted permanent-magnet synchronous machine drives," *IEEE Trans. Energy Convers.*, vol. 14, no. 4, pp. 1043–1050, Dec. 1999.

[6] V. Petrović, R. Ortega, A. Stanković, and G. Tadmor, "Design and implementation of an adaptive controller for torque ripple minimization in PM synchronous motors," *IEEE Trans. Pow. Electron.*, vol. 15, no. 5, pp. 871–880, Sept. 2000.

[7] A. P. Wu and P. L. Chapman, "Simple expressions for optimal current waveforms for permanent-magnet synchronous machine drives," *IEEE Trans. Energy Convers.*, vol. 20, no. 1, pp. 151–157, March 2005.

[8] P. Mattavelli, L. Tubiana, and M. Zigliotto, "Torque-ripple reduction in PM synchronous motor drives using repetitive current control," *IEEE Trans. Pow. Electron.*, vol. 20, no. 6, pp. 1423–1431, Nov. 2005.

[9] C. Marchand and A. Razek, "Optimal torque operation of digitally controlled permanent magnet synchronous motor drives," *Proc. Inst. Elect. Eng. B*, vol. 140, no. 3, pp. 232–240, May 1993.

[10] A. Madani, J. Barbot, F. Colamartino, and C. Marchand, "Reduction of torque pulsations by inductance harmonics identification of a permanent-magnet synchronous machine," in *Proc. IEEE CCA'95*, Albany, NY, Sept. 1995, pp. 787–792.

[11] F. Colamartino, C. Marchand, and A. Razek, "Torque ripple minimization in permanent magnet synchronous servodrive," *IEEE Trans. Energy Convers.*, vol. 14, no. 3, pp. 616–621, Sept. 1999.

[12] A. Piippo and J. Luomi, "Adaptive observer combined with HF signal injection for sensorless control of PMSM drives," in *Proc. IEEE IEMDC'05*, San Antonio, TX, May 2005, pp. 674–681.

[13] ——, "Inductance harmonics in permanent magnet synchronous motors and reduction of their effects in sensorless control," in *Proc. ICEM/2006*, Chania, Greece, Sept. 2006, in press.

[14] A. Piippo, M. Hinkkanen, and J. Luomi, "Analysis of an adaptive observer for sensorless control of PMSM drives," in *Proc. IEEE IECON'05*, Raleigh, NC, Nov. 2005, pp. 1474–1479.

[15] L. Springob and J. Holtz, "High-bandwidth current control for torque-ripple compensation in PM synchronous machines," *IEEE Trans. Ind. Electron.*, vol. 45, no. 5, pp. 713–721, Oct. 1998.

[16] T. Jahns, G. Kliman, and T. Neumann, "Interior permanent-magnet synchronous motors for adjustable-speed drives," *IEEE Trans. Ind. Applicat.*, vol. 22, no. 4, pp. 738–747, July/Aug. 1986.

[17] H. Song and K. Nam, "Dual current control scheme for PWM converter under unbalanced input voltage conditions," *IEEE Trans. Ind. Electron.*, vol. 46, no. 5, pp. 953–959, Oct. 1999.

[18] F. Briz del Blanco, M. W. Degner, and R. D. Lorenz, "Dynamic analysis of current regulators for AC motors using complex vectors," *IEEE Trans. Ind. Applicat.*, vol. 35, no. 6, pp. 1424–1432, Nov./Dec. 1999.

[19] J. K. Pedersen, F. Blaabjerg, J. W. Jensen, and P. Thogersen, "An ideal PWM-VSI inverter with feedforward and feedback compensation," in *Proc. EPE'93*, vol. 5, Brighton, UK, Sept. 1993, pp. 501–507.